Journal of King Saud University – Science 32 (2020) 1382–1389

Contents lists available at ScienceDirect

Journal of King Saud University – Science

journal homepage: www.sciencedirect.com

Original article

Effect of fuel content on nonlinear optical and antibacterial activities of $Zn/Cu/Al_2O_4$ nanoparticles prepared by microwave-assisted combustion method

A. Lakshmanan [a], P. Surendran [a], S. SakthyPriya [a], K. Balakrishnan [a], Tejaswi Ashok Hegde [b], G. Vinitha [b], G. Ramalingam [c], B. Ravindran [d,e,f,*], S.W. Chang [d], M.S. Elshikh [g], A.H. Mahmoud [h], D.A. Al Farraj [g], P. Rameshkumar [a,*]

[a] Crystal and Nanomaterials Lab, Department of Physics, Periyar E.V.R. College (Autonomous), Tiruchirappalli 620 023, Tamilnadu, India
[b] Division of Physics, School of Advanced Sciences, VIT Chennai, Chennai 600 127, Tamilnadu, India
[c] Department of Nanoscience and Technology, Alagappa University, Karaikudi 630 003, Tamilnadu, India
[d] Department of Evironmental Energy and Engineering, Kyonggi University, Youngtong Gu, Suwon 16227, South Korea
[e] Department for Management of Science and Technology Development, Ton Duc Thang University, Ho Chi Minh City, Vietnam
[f] Faculty of Environment and Labour Safety, Ton Duc Thang University, Ho Chi Minh City, Vietnam
[g] Department of Botany and Microbiology, College of Science, King Saud University, Riyadh 11451, Saudi Arabia
[h] Department of Zoology, College of science, King Saud University, Riyadh, Saudi Arabia

ARTICLE INFO

Article history:
Received 30 September 2019
Revised 18 November 2019
Accepted 21 November 2019
Available online 28 November 2019

Keywords:
$Zn/Cu/Al_2O_4$ nanoparticles
Combustion method
Optical properties
Luminescence
Z-scan
Antibacterial activity

ABSTRACT

Nonlinear optical nanoparticles of $Zn/Cu/Al_2O_4$ were synthesized by microwave-assisted combustion method with different fuel to oxidizer ratio. And, these nanoparticles were characterized by various analytical techniques to examine their suitability in fascinating applications. XRD results enunciate that the nanoparticle crystallizes in *cubic spinel* structure. The morphology and quantitative chemical compositions of Zn, Cu, Al and O elements were obtained from SEM with EDAX analysis. The prepared compound was confirmed by FTIR spectrum. The optical energy bandgaps are studied from UV–Vis absorption spectra. The luminescence emission peaks are observed at 371 nm (Violet), 425 nm (violet), 471 nm (blue) and 637 nm (red). In the application point of view from the Z-scan technique, the third order nonlinear optical parameters such as nonlinear refractive index (n_2), nonlinear absorption coefficient (β), and third-order nonlinear susceptibility (χ^3) of title compound are calculated. For biological application, the antibacterial activities were tested against *Bacillus cereus, Staphylococcus aureus, Shigella flexneri, and Vibrio cholera* bacterial species by measuring the inhibition zone. Existing results point out that the synthesized $Zn/Cu/Al_2O_4$ nanoparticles are possible candidates for photonics devices, optical switches, optical limiting and also for pharmaceutical applications.

1. Introduction

At the moment, researchers working in the field of nanotechnology are focusing to find promising materials for plenty of applications like telecommunication, optoelectronics, biological and nonlinear optics (Rithesh Raj et al., 2015). Nonlinear optics has a great value and various applications in optical switching, image transmission, data storage and signal processing (Zhang et al., 2008). For the past two decades, number of studies was made on NLO properties of novel materials because of its vital applications (Zhang and Wang, 2017). Recent research on nonlinear optics directs on nanomaterial's that will be used to fabricate advanced novel optical devices with minimum expense and more efficiency (Yugandhar et al., 2017). Many earlier findings revealed the structural and physical characteristics articulated by ternary metal oxide complex with a spinel structure (Mao et al., 2005). These spinel structure compounds showed high thermal and chemical sta-

* Corresponding authors.
E-mail addresses: kalamravi@gmail.com, balasubramani.ravindran@tdtu.edu.vn (B. Ravindran), rameshkumarevr@gmail.com (P. Rameshkumar).

Peer review under responsibility of King Saud University.

Production and hosting by Elsevier

https://doi.org/10.1016/j.jksus.2019.11.031
1018-3647/

bility and low temperature sinterability. Also, showed low surface acidity, high quantum yields, better diffusion and hydrophobic behavior gained much more attention in last two decades (Zawadzki, 2006). The spinels are class of binary transition metal oxides of the form AB_2O_4 with varied structural and potential uses in applications in the field of materials science (Zhang et al., 2011). Among the various spinel structures, zinc aluminate ($ZnAl_2O_4$) has multidisciplinary applications like optical materials, electrical, catalyst support, ceramic materials and optical coating or host matrix (Pathak et al., 2014). $ZnAl_2O_4$ is a direct wide bandgap semiconductor (3.8 eV), which is used for wide range of applications especially in optoelectronic devices that are operated in the UV region (Wang et al., 2005). Zinc aluminate nanoparticles can be prepared by variety of methods as given by (Cornu et al., 2014). Compared to other methods, one interesting and novel technique is the microwave-assisted combustion method to synthesize nanomaterials. This method is eco-friendly, very high reaction rate, energy saving method, rapid heating and very short reaction time. Investigation about large nonlinear optical properties of these spinel structure nanomaterials is still one of the important works concerning nonlinear optical applications (Panoiu et al., 2018).

Hence, microwave-assisted combustion method was used to synthesize Zn/Cu/Al_2O_4 nanoparticles with different fuel to oxidizer ratio. These synthesized nanoparticles were characterized by various analytical methods and also tested antibacterial activity. The novelty of this work is to determine the nonlinear properties of Zn/Cu/Al_2O_4 nanoparticles in order to confirm their suitability in optical limiting device and also to test the antibacterial activity against foodborne pathogens.

2. Experimental procedures

2.1. Materials

Starting metal precursors which are used in this experiment are Zinc nitrate hexahydrate (Zn $(NO_3)_2{\cdot}6H_2O$), Copper nitrate hexahydrate ($Cu(NO_3)_2{\cdot}6H_2O$), and Aluminum nitrate monohydrate (Al $(NO_3)_3{\cdot}9H_2O$) which act as oxidizer and glycine (NH_3 COOH CH_2) as a fuel.

2.2. Methods

The $Zn_{0.96}Cu_{0.04}Al_2O_4$ nanoparticles were prepared via microwave-assisted combustion method with various fuel to oxidizer ratio such as, stoichiometric (S), fuel lean (L), and rich (R). The constituents in the desired fuel to oxidizer ratio in stoichiometric conditions were suspended in double distilled water (15 mL). The mixture was vigorously stirred at 90 °C for 30 mins until it forms a highly viscous gel, then it was kept in a microwave oven with the output power of 800 Watts. In the early stage, the gel was effervescence and burst into flames with enormous amount of gases which result in yielding of foamy and porous structure. Finally, the yield was collected and calcination was done at 700 °C for 6 h. The same experimental procedure was continued for the remaining fuel to oxidizer ratios like fuel lean and rich.

2.3. Combustion mechanism

Bipropellant chemistry, microwave-assisted combustion synthesis relies on an exothermic redox reaction between glycine and metal nitrate. In this combustion process, metal nitrates like Zn, Cu and Al nitrate function as oxidizers, whereas glycine functions as a reducer. Typically, valency for the elements are Zinc (+2), Copper (+2), Aluminum (+3), Hydrogen (+1), Carbon (+4) and Oxygen (-2). Generally, element nitrogen is assumed to be zero. Hence, equivalent capacity are Zinc nitrate (−10), Copper nitrate (−10), Aluminum nitrate (−15) and glycine (+9). For a stoichiometric ratio, we need 0.96 (−10) + 0.04 (−10) + 2 (−15) + n (+9) = 0, which provides n = 4.44 mol of glycine. Jain et al. (1981) have calculated the nitrate to glycine ratio which is represented by $(\varnothing_e)$ using the relation,

$$\varnothing_e = \frac{\Sigma(\text{coefficient of oxidizing elements}) \times (\text{valency})}{(-1)\Sigma(\text{coefficient of reducing elements}) \times (\text{valency})} \quad (1)$$

The coefficients of reducing element for the oxidizer to fuel ratios are $(\varnothing_e > 1)$ for fuel lean, $\varnothing_e < 1)$ for fuel rich and $(\varnothing_e = 1)$ for stoichiometric. The combustion reaction to prepare $Zn_{0.96}Cu_{0.04}Al_2O_4$ reaction is expressed as follows.

1. Fuel lean ($\varnothing_e$ = 0.5, Fuel/Nitrate ratio = 0.74)

$$0.04\,Cu(NO_3)_2.3H_2O + 0.96\,Zn(NO_3)_2.6H_2O + 2\,Al(NO_3)_3.9H_2O + 2.22\,NH_2COOH\,CH_2 \times \xrightarrow{\Delta} Zn_{0.96}Cu_{0.04}Al_2O_4 + 4.44\,CO_2 \uparrow + 29.43\,H_2O \uparrow + 5.11\,N_2 \uparrow + 5.005\,O_2 \quad (2)$$

It shows that more amount of oxygen released to the surrounding environment.

2. Fuel stoichiometric ($\varnothing_e$ = 1, Fuel/Nitrate ratio = 1.48)

$$0.96\,Zn(NO_3)_2.6H_2O + 0.04\,Cu(NO_3)_2.3H_2O + 2\,Al(NO_3)_3.9H_2O + 4.44\,NH_2COOH\,CH_2 \times \xrightarrow{\Delta} Zn_{0.96}Cu_{0.04}Al_2O_4 + 8.88\,CO_2 \uparrow + 34.98\,H_2O \uparrow + 6.22\,N_2 \uparrow \quad (3)$$

From the reaction, it is very clear that oxidizing fuel reacts with the oxygen from metal nitrate completely and for the complete reaction, no heat exchange is generally required.

3. Fuel rich ($\varnothing_e$ = 1.5, Fuel/Nitrate ratio = 2.22)

$$0.04\,Cu(NO_3)_2.3H_2O + 0.96\,Zn(NO_3)_2.6H_2O + 2\,Al(NO_3)_3.9H_2O + 6.66\,NH_2COOHCH + 4.982\,O_2 \times \xrightarrow{\Delta} Zn_{0.96}Cu_{0.04}Al_2O_4 + 13.32\,CO_2 \uparrow + 40.53\,H_2O \uparrow + 7.33\,N_2 \uparrow \quad (4)$$

It is very clear, to finish the combustion process, further oxygen is needed from the atmosphere.

2.4. Instrumentation

The PXRD analysis was performed to characterize the synthesized nanoparticles using XPERTPRO X-ray powder diffractometer system. The 2θ range analyzed between 10°-80°, the scan speed was set as 0.1 min^{-1} The morphologies were observed by SEM (Make: CAREL ZEISS, Model: EVO 18). FTIR spectra were analyzed using a Perkin–Elmer spectrophotometer in the range of 400–4000 cm^{-1} at room temperature. The linear optical absorption and electronic transition of the nanoparticles were investigated using a UV–Visible spectrophotometer (scan range: 200 to 800 nm). The luminescence spectra was recorded in the spectrofluorophotometer (shimadzu/RF 6000).

2.5. Z-Scan measurement

In this experiment, $Zn_{0.96}Cu_{0.04}Al_2O_4$ nanoparticles were investigated for third order nonlinear optical properties using CW laser (532 nm, 100 mW) as excitation source. Initially, the prepared $Zn_{0.96}Cu_{0.04}Al_2O_4$ nanoparticles were dispersed in ethylene glycol by ultra-sonication with transmittance nearly 65%. The dispersed solution was taken in 1 mm cuvette and was mounted on a trans-

lation stage that was slowly shifted into the laser propagation pathway. The corresponding far field transmittance was observed by a photodetector.

2.6. Antibacterial activity

Nanoparticles were subjected for antimicrobial activity studies using disc diffusion method (Vijayalakshmi and Dhanasekaran, 2018) against various bacterial pathogens on Mueller Hinton agar plate. The medium that supports the growth inhibition of bacterial cultures were maintained at 37 °C using an incubator. The sterilized petri dish that was used in the experiment was inhibited at 120 °C for 30 mins. The synthesized nanomaterial was dispersed in deionized water. The dispersed solution was loaded on sterile dishes on Mueller Hinton agar plate seeded with bacteria. The petri plates were incubated for 18 h. After 18 h, the results were observed and the diameter of the zone was measured (mm).

3. Results and discussions

3.1. PXRD analysis

The XRD patterns obtained for the $Zn_{0.96}Cu_{0.04}Al_2O_4$ nanoparticles are described in Fig. 1 (a, b, c). It is clear that the diffraction peaks corresponding to the crystallography planes of (2 2 0), (3 1 1), (4 0 0), (3 3 1), (4 2 2), (5 1 1), (4 4 0), (6 2 0), and (5 3 3) are in accordance with JCPDS data (Card No:73-1961). These characters confirmed the presence of cubic spinel structure. However, PXRD pattern did not show any secondary phase diffraction peaks. Debye-Scherrer's formula was used for the determination of the mean crystallite size (D) as suggested by Pathak et al. (2016).

$$D = k\lambda/\beta COS\theta \quad (5)$$

where, k is the shape factor, λ denotes wavelength (WL) of X-ray radiation (λ = 0.15406 nm), θ denotes diffraction angle and β denotes full width half maximum (FWHM) of the observed peak. The mean crystallite sizes for different fuel ratio are 25 nm (L), 30 nm (S)and 32 nm (R), which shows good crystallinity. Thus the estimated average crystallite size responds significantly with the fuel to oxidizer ratio. The lattice parameter of as-prepared materials from the most intense peak (3 1 1) plane was calculated using the following formula as suggested by Yadav et al. (2018).

$$a = d_{hkl}\sqrt{h^2 + k^2 + l^2} \quad (6)$$

where d_{hkl} denotes inter planar distance, and miller indices are termed as, h, k and l. The analyzed values of lattice parameter were found to be 8.0542 Å (L), 8.05167 Å (S), and 8.0491 Å (R) for as-prepared $Zn_{0.96}Cu_{0.04}Al_2O_4$ nanoparticles, respectively.

3.1.1. Williamson - Hall analysis

Williamson-Hall (W-H) equation, to calculate the lattice strain is,

$$\beta\cos\theta = 4\varepsilon\sin\theta + K\lambda/D \quad (7)$$

where, ε denotes the lattice strain of materials. Fig. 2 (a, b, c) exhibits the plot drawn for 4sinθ*Vs* βcosθ. The calculated lattice strain values are −4.80 (L), 1.17 (S) and 5.66 (R). As fuel to oxidizer ratio increases, the lattice strain values changes from negative to positive strain (Fig. 2). The negative strain value indicates the presence of compressive strain and positive values specify tensile strain in the material. The equation$\delta = 1/D^2$ was used to calculate dislocation density (Aly et al., 2016) and values for fuel lean, stoichiometric and rich are 1.6000 × 10^{15}, 1.1111 × 10^{15} and9.7656 × 10^{14} (Lines/m^2).

3.2. Morphological studies

The morphology of the nanoparticles are analyzed using SEM and are shown in Fig. 3 (a, b, c). The nanoparticles are accompanied by agglomeration and coalescence. In Fig. 3a, it is seen that cubic structure is formed with some nanoparticles deposited on the structure. In Fig. 3b, cubic spinel structure is obtained with some agglomeration. Fig. 3cshows the spongy network structureformed in the nanoparticles. SEM images, reveals slight morphological difference in different size agglomerates covered by smaller particlesdue to selection of fuel.

3.3. Compositional analysis

EDAX was carried out to confirm the elemental composition in the synthesized nanoparticles for fuel (L, S & R) is depicted in the Fig. 4 (a, b, c). The corresponding peaks of the elements O, Al, Zn and Cu were determined for the synthesized nanoparticles. The elements are well distributed and without any characteristic impurity peak indicating the purity of prepared materials. The content of Zn, Cu, Al and O differs with fuel to oxidizer ratio. Moreover, the atomic ratio significantly decreases with increase in the fuel to oxidizer ratio.

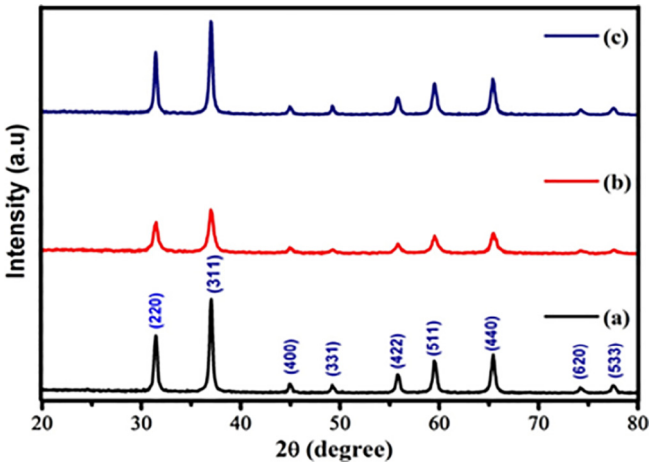

Fig. 1. The synthesis $Zn_{0.96}Cu_{0.04}Al_2O_4$ nanoparticles for different fuel ratios (a) Fuel lean, (b) Fuel stoichiometric (c) Fuel rich: (1) XRD pattern.

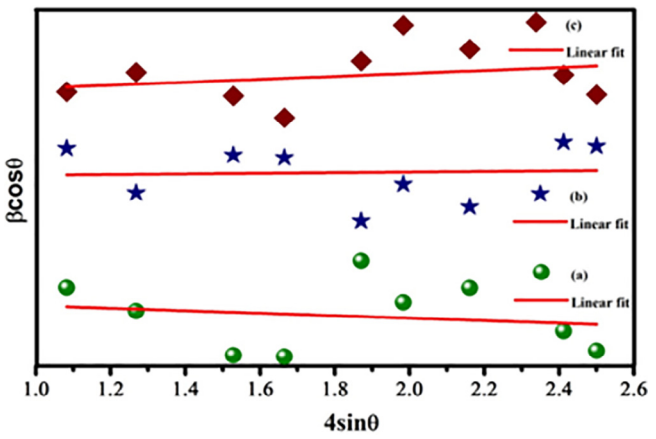

Fig. 2. The synthesis $Zn_{0.96}Cu_{0.04}Al_2O_4$ nanoparticles for different fuel ratios (a) Fuel lean, (b) Fuel stoichiometric (c) Fuel rich: (2) W-H plots.

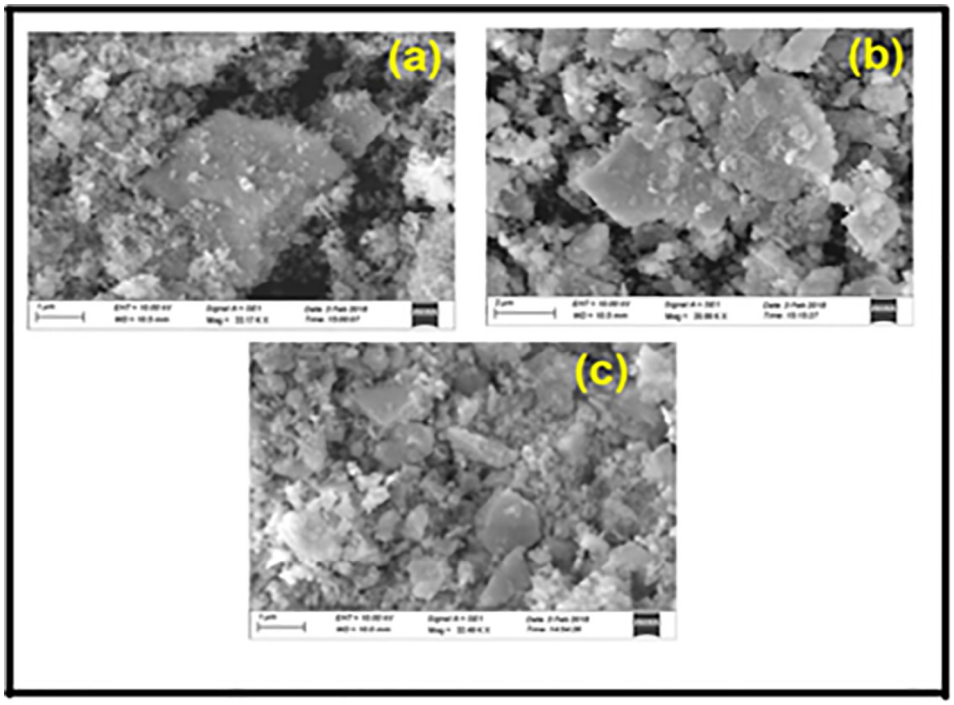

Fig. 3. The synthesis $Zn_{0.96}Cu_{0.04}Al_2O_4$ nanoparticles for different fuel ratios (a) Fuel lean, (b) Fuel stoichiometric (c) Fuel rich: (3) SEM images.

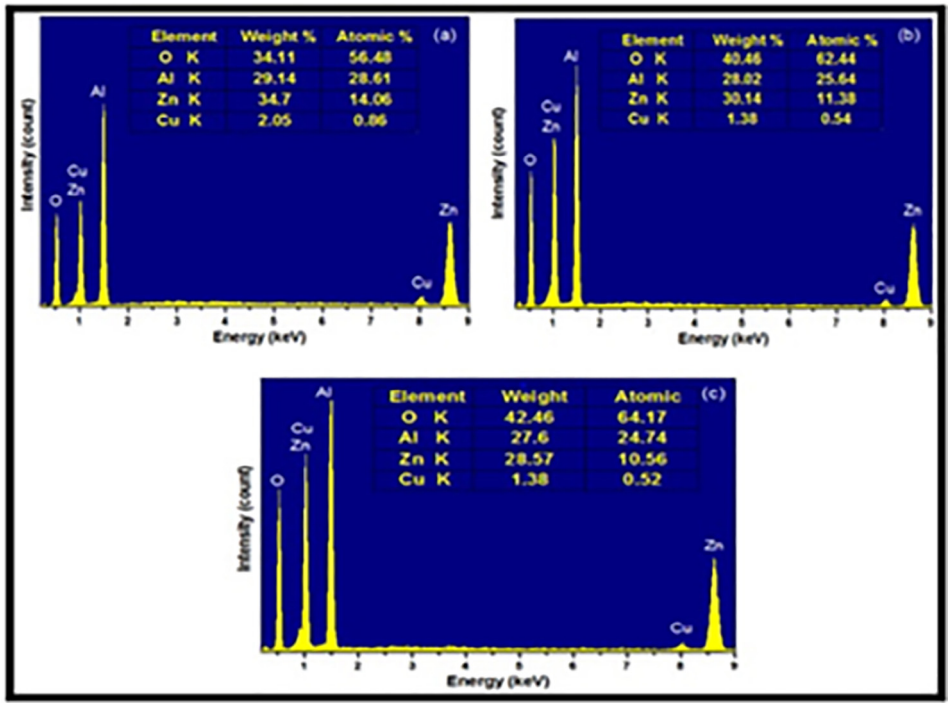

Fig. 4. The synthesis $Zn_{0.96}Cu_{0.04}Al_2O_4$ nanoparticles for different fuel ratios (a) Fuel lean, (b) Fuel stoichiometric (c) Fuel rich: (4) EDAX spectra.

3.4. FTIR analysis

The chemical bonding and functional groups of synthesized nanoparticles were identified by FTIR spectrum. The infrared spectra of the prepared sample are depicted in Fig. 5 (a, b, c). The absorption band at 3443 cm^{-1} and 1633 cm^{-1} could be assigned to O–H stretching vibration due to water (H_2O) adsorption (Theophil Anand et al., 2019). A band observed at 2924 cm^{-1} could assign to C–H stretching vibration. Also observed a band at the wave number 2340 cm^{-1} could attributed to stretching vibration modes of CO_2 molecule in the air. The peak at 1712 cm^{-1} is due to the C = O carbonyl group. In this present work, metal–oxygen stretching frequencies appear as three main peaks between 400 and 800 cm^{-1}. The bands observed at 667 cm^{-1}, 558 $cm^{-1}$and 501 cm^{-1} are mainly attributed to intrinsic metal stretching vibration of theM_{tetra} – Ositeand stretching M_{octra} – Osite (Ahmed et al.,

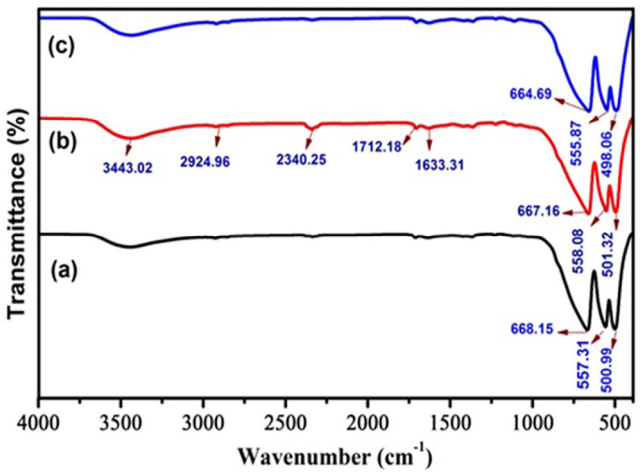

Fig. 5. The synthesis $Zn_{0.96}Cu_{0.04}Al_2O_4$ nanoparticles for different fuel ratios (a) Fuel lean, (b) Fuel stoichiometric (c) Fuel rich: (5) FTIR spectra.

2011). These bands in the formation of crystallite phase spinel structure which is in accordance with the XRD results.

3.5. Optical studies

The optical absorption spectra are shown in Fig. 6a for the prepared nanoparticles have maximum absorption edge around 331 nm (L), 335 nm (S) and 337 nm (R). There are small variations in the absorption edges and also intensity of edges increase with increase in F/O ratios of glycine. The optical energy bandgap were calculated by the Tauc's equation (Bhaumik et al., 2014),

$$\alpha h\upsilon = A\left(h\upsilon - E_g\right)^n \tag{8}$$

where, E_g is the energy bandgap, $h\upsilon$ is the incident photon energy, n = 2 and 1/2 for indirect and direct transitions respectively. The optical bandgap of the nanoparticles are given in Fig. 6b. In the present case, optical bandgap values are found to be (L) 3.74eV, (S) 3.71eV and (R) 3.68 eV respectively. The energy bandgap is high for the smaller crystallite size compared to high crystallite size. These wide bandgaps reveal that the synthesized nanoparticles are highly suitable for various uses as, nonlinear, optoelectronic and photocatalysis applications (Mobeen et al., 2019).

3.6. Luminescence analysis

Luminescence spectra analysis was performed and the results were shown in Fig. 7. The entire sample exhibiting emission peaks at 371, 425, 471 and 637 nm are found in the luminescence spectra under the excitation wavelength of λ_{exc} = 330 nm. In this study, violet emission peaks were observed at 371 and 425 nm and this characteristic emission peaks were previously determined by Geetha Devi and Sakthi Velu (2016). The blue emission peaks were observed near 471 nm and this kind of blue emission peak was previously reported by Vijayaprasath et al. (2015). A red emission peak was observed at 637 nm mainly due to surface state and deep trap emission. The luminescence emission intensity is observed to significantly decrease with high increase in fuel to oxidizer ratio and there is also a slight peak shift as depicted in the spectrum. The luminescence emission peak shift is due to the variation position of the defect levels within the bandgap. These results indicate that, it has a potential application in monochromatic laser and other optoelectronic devices (Karthik et al., 2017).

3.7. Z-Scan analysis

This technique has been developed by Sheik-bahae et al. (1989) to determine both the nonlinear absorption coefficient and nonlinear refractive index for the prepared nanoparticles. The recorded closed aperture and open aperture Z-Scan curves are described in Fig. 8a and b respectively. In this study, open aperture Z-Scan curves were determined. This observation revealed that the sample exhibit the self-defocusing nonlinearity and reverse saturable absorption (RSA). The nonlinear optical parameters are calculated using standard relations (Yugandhar et al., 2017). The third order nonlinear optical susceptibility ($\chi^{(3)}$) can be estimated using,

$$\mathrm{Re}\chi^{(3)} = \frac{10^{-4}\left(\varepsilon_0 C^2 n_0^2 n_2\right)}{\pi}(\mathrm{cm}^2/\mathrm{W}) \tag{9}$$

$$\mathrm{Im}\chi^{(3)} = \frac{10^{-2}\left(\varepsilon_0 C^2 n_0^2 \lambda\beta\right)}{4\pi^2}(\mathrm{cm}/\mathrm{W}) \tag{10}$$

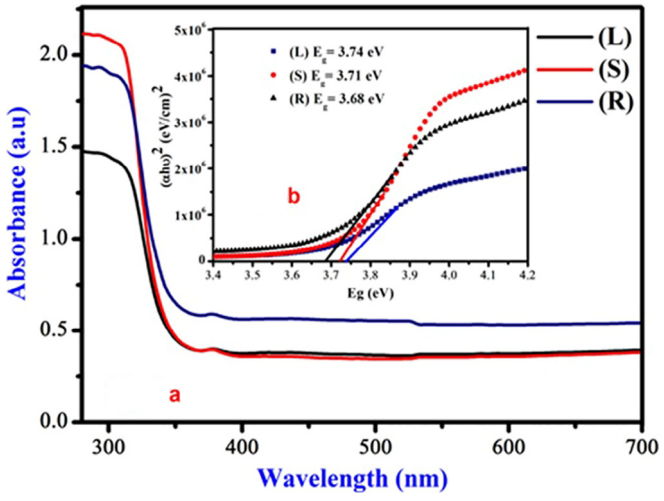

Fig. 6. The synthesis $Zn_{0.96}Cu_{0.04}Al_2O_4$ nanoparticles for different fuel ratios (a) Fuel lean, (b) Fuel stoichiometric (c) Fuel rich: (6a) UV–Vis absorption spectra (6b) Optical bandgap.

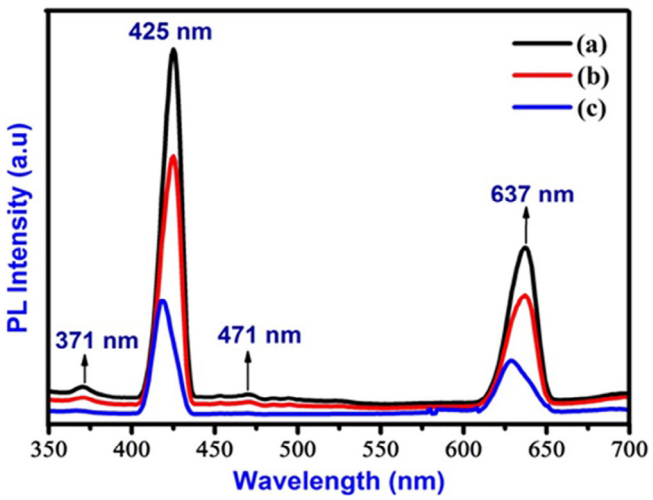

Fig. 7. The synthesis $Zn_{0.96}Cu_{0.04}Al_2O_4$ nanoparticles for different fuel ratios (a) Fuel lean, (b) Fuel stoichiometric (c) Fuel rich: (7) Emission spectrum.

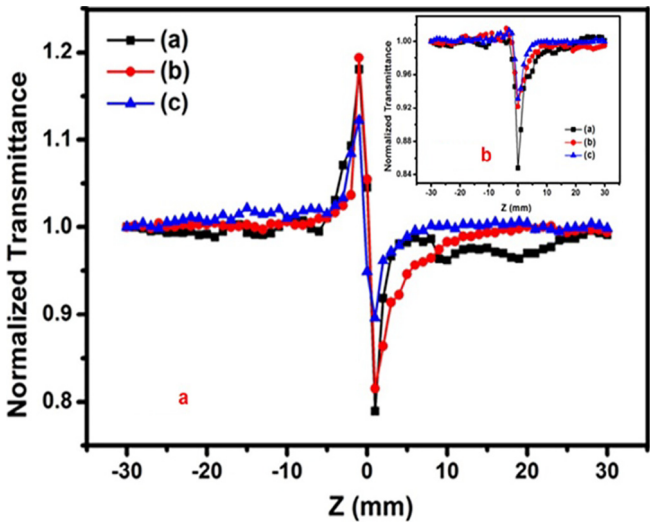

Fig. 8. The synthesis $Zn_{0.96}Cu_{0.04}Al_2O_4$ nanoparticles for different fuel ratios (a) Fuel lean, (b) Fuel stoichiometric (c) Fuel rich: (8a) Closed aperture (8b) Closed aperture Z-scan analysis.

Hence, ε_0 is the permittivity of vacuum (8.854×10^{-12}F/m), n_0 is the linear refractive index of the nanomaterial and c is the velocity of the light in vacuum (3×10^8 m/s). Then, the third order nonlinear optical susceptibility($\chi^{(3)}$) of the prepared nanoparticles can be calculated from

$$X^{(3)} = \sqrt{\left(\mathrm{Re}X^{(3)}\right)^2 + \left(\mathrm{Im}X^{(3)}\right)^2} \quad (11)$$

The analyzed parameters of third-order nonlinear optical nonlinearity are described in Table 1. The open aperture Z-Scan curves of this study clearly illustrate decrease in transmission with significant increase in the input intensity. This finding indicates the availability of RSA and has been previously reported by Henari (2001). The obtained results confirm that $Zn_{0.96}Cu_{0.04}Al_2O_4$ nanoparticles are suitable material for optical limiting device applications.

3.8. Antibacterial activity

The synthesized nanoparticles were evaluated against foodborne bacterial pathogens such as, *Staphylococcus aureus*, *Bacillus cereus, Shigella flexneri, Vibrio cholerae* bacteria. Nanoparticles showed activity against these bacterial pathogens (Fig. 9). Photograph of antibacterial activity of $Zn_{0.96}Cu_{0.04}Al_2O_4$ nanoparticles is shown in Fig. 10. By the formation of zone of inhibition, the

Table 1
Third order measurement values of prepared $Zn_{0.96}Cu_{0.04}Al_2O_4$ nanoparticles for different fuel to oxidizer ratio.

Parameters	Fuel Lean	Fuel Stoichiometric	Fuel Rich
Linear absorption coefficient (α)	85.441	81.756	75.999
Linear refractive index (n_0)	1.3602	1.3526	1.3412
Nonlinear refractive index $n_2 \times 10^{-9}$cm^2/W	2.4615	2.1503	1.4224
Nonlinear absorption coefficient (β)×10^{-4} cm/W	1.2949	0.6632	0.5803
Real part $(\chi)^{(3)} \times 10^{-7}$esu	1.1557	0.9984	0.6493
Imaginary part of $(\chi)^{(3)} \times 10^{-8}$esu	2.5752	1.3042	1.1221
Third order nonlinear susceptibility $(\chi)^{(3)} \times 10^{-7}$esu	1.1840	1.0068	0.6589

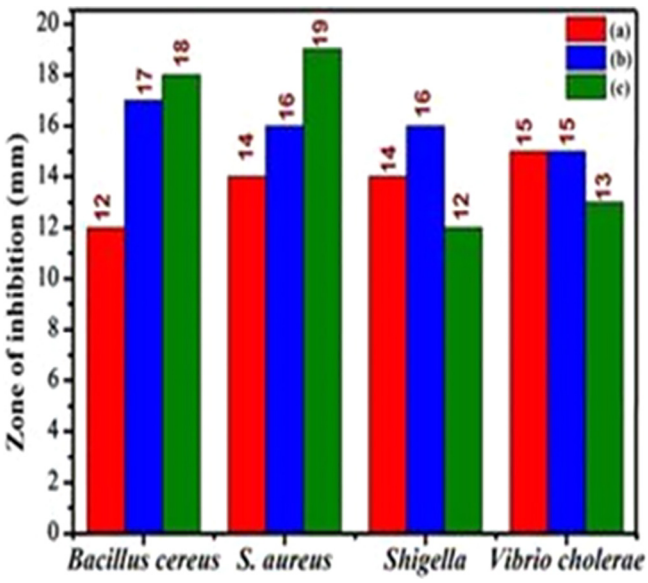

Fig. 9. The antibacterial activity of synthesized nanoparticles for different fuel ratios (a) Fuel lean, (b) Fuel stoichiometric (c) Fuel rich: (9) zone of inhibition.

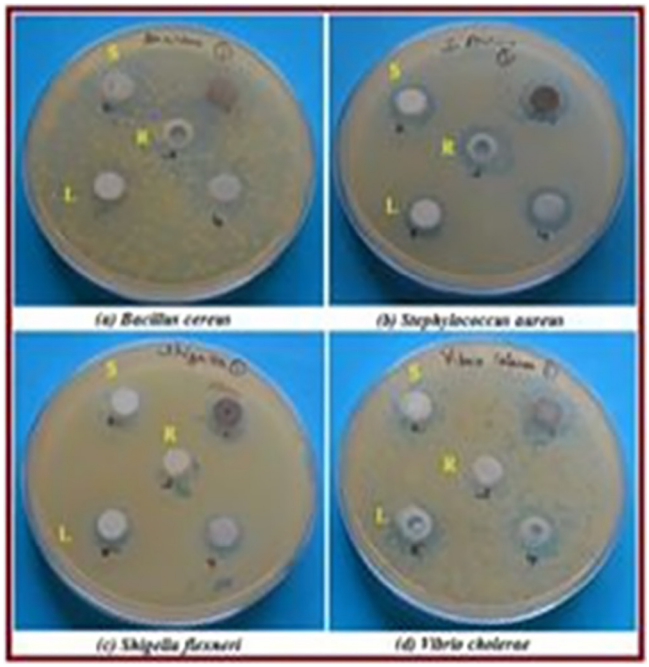

Fig. 10. The antibacterial activity of synthesized nanoparticles for different fuel ratios (a) Fuel lean, (b) Fuel stoichiometric (c) Fuel rich: (10) Antibacterial activity plate photos and.

results prove that the samples have good antibacterial activity. The important mechanism of metal oxide in antimicrobial property is the disruption of cell wall by various mechanisms, including generation of reactive oxygen species (ROS) which causes cell disruption (Karthik et al., 2019a).

Fig. 11 illustrates the antibacterial mechanism of $Zn/Cu/Al_2O_4$ nanoparticles. The process involved attraction of positive charged heavy metal ions (Zn^{2+}, Cu^{2+} and Al^{3+}) with negative charged cell wall and penetrate into the cell wall. Certain bacteria produce ROS production in host organism, including human and may cause cancer (Sadiq et al., 2009). $Zn/Cu/Al_2O_4$ nanoparticles have the capacity to inhibit the production of ROS in bacteria and protect

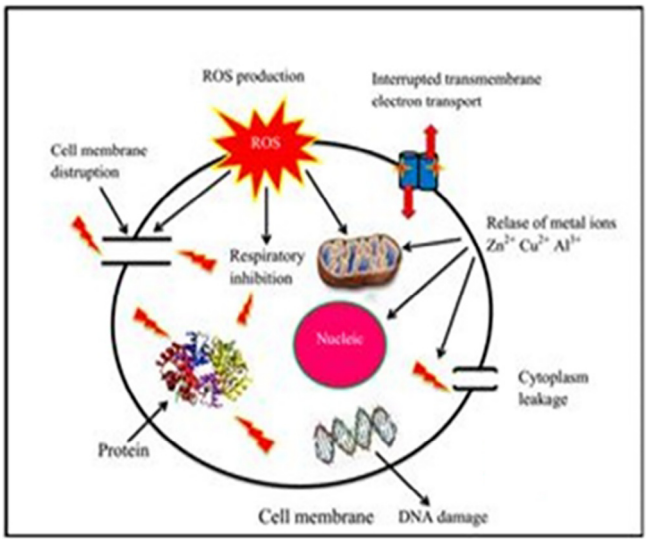

Fig. 11. The antibacterial activity of synthesized nanoparticles for different fuel ratios (a) Fuel lean, (b) Fuel stoichiometric (c) Fuel rich: (11) antibacterial mechanism.

mammalian cell damage (Parham et al., 2016). Hence, the synthesized nanoparticles are efficient material against the foodborne pathogens which are suitable for medical devices and paramedical applications (Karthik et al., 2019). The prepared $Zn/Cu/Al_2O_4$ nanoparticles have potential antibacterial activity than other metal oxides (Table 2).

Table 2
Antibacterial activities of $Zn/Cu/Al_2O_4$ nanoparticles were compared with various metal oxide nanoparticles.

Bacteria species	Materials	Zone of inhibition (mm) ± standard deviation	References
Staphylococcus aureus	NiO	10	(Karthik et al., 2018)
	Al_2O_3	12	(Manyasree et al., 2018)
	MgO	12 ± 0.10	(EL-Moslamy et al., 2018)
	CuO	9 ± 0.8	(Yugandhar et al., 2017)
	ZnO	11 ± 0.23	(Zare et al., 2019)
	Ni-ZnO	12	(Brintha and Ajitha, 2016)
	Al-ZnO	12	(Brintha and Ajitha, 2016)
	$NiFe_2O_4$	6.4	(Allafchian et al., 2016)
	$NiFe_2O_4$@Ag	12.5	(Allafchian et al., 2016)
	$Zn/Cu/Al_2O_4$	**19**	**Present work**
Bacillus cereus	MgO	15 ± 0.03	(EL-Moslamy et al., 2018)
	Ni-ZnO	8	(Brintha and Ajitha, 2016)
	Al-ZnO	12	(Brintha and Ajitha, 2016)
	$NiFe_2O_4$	6.4	(Allafchian et al., 2016)
	$NiFe_2O_4$@Ag	11.5	(Allafchian et al., 2016)
	$Zn/Cu/Al_2O_4$	**18**	**Present work**
Vibrio cholera	ZrO_2	12	(Karthik et al., 2019c)
	CdO	12	(Karthik et al., 2017)
	CdO-MgO	12	(Karthik et al., 2019a)
	$Zn/Cu/Al_2O_4$	15	**Present work**
Shigellaflexneri	Ta_2O_5	10 ± 0.2	(Nagaraju et al., 2019)
	MgO	10 ± 2.3	(EL-Moslamy et al., 2018)
	TiO_2	12	(Karthik et al., 2019d)
	$Zn/Cu/Al_2O_4$	**16**	**Present work**

4. Conclusion

In our study, $Zn_{0.96}Cu_{0.04}Al_2O_4$ eco-friendly microwave-assisted combustion method was used for the synthesis of nanoparticles. These were characterized by various analytical techniques and antibacterial activities were assayed. The synthesized nanoparticles showed cubic spinel structure. The morphological and elemental composition was confirmed by SEM and EDAX. The optical bandgap is found to be 3.74 eV (L), 3.71 eV (S) and 3.68 eV (R) with absorption wavelength at 331 (L), 335 (S) and 337 nm (R) respectively. The luminescence nature of the nanoparticles was studied by luminescence spectra which can be effectively used in monochromatic laser and also in optoelectronic devices. The third order NLO properties results enunciate that the sample can be used in nonlinear optical limiting device applications. The sample inhibits the growth of various foodborne pathogens and exhibits potential activity against both Gram-positive and Gram-negative bacteria. The above experimental result reveals that, $Zn_{0.96}Cu_{0.04}$-Al_2O_4 nanoparticles provide potential applications in photonic devices and antibacterial activity which restricts the selected bacterial growth confirms the suitability in pharmaceutical applications.

Declaration of Competing Interest

The authors declare that they have no known competing financial interests or personal relationships that could have appeared to influence the work reported in this paper.

Acknowledgements

One of the authors A. Lakshmanan wish to thank the UGC-RGNF [F1-17.1/2016-17/RGNF-2015-17-SC-TAM-21802] and P. Surendran is grateful to UGC-NFHE [F1-17.1/2015-16/NFST-2015-17-ST-TAM-1335] New Delhi, India, for the financial support. G. Ramalingam acknowledges financial support from RUSA 2.0, Grant/Award Number: RUSA 2.0 grant No.F.24-51/2014-U, Policy (TN Multi-Gen) & DST-SERB/2016/198 for instrumentation facility used at Alagappa University, Karaikudi. The authors extend their appreciation to The Researchers supporting project number (RSP-2019/108) King Saud University, Riyadh, Saudi Arabia. This work was supported by the Korea Institute of Energy Technology Evaluation and Planning(KETEP) and the Ministry of Trade, Industry & Energy (MOTIE) of the Republic of Korea (No. 20194110300040).

References

Ahmed, F., Kumar, S., Arshi, N., Anwar, M.S., Su-Yeon, L., Kil, G.S., Park, D.W., Koo, B. H., Lee, C.G., 2011. Preparation and characterizations of polyaniline (PANI)/ZnO nanocomposites film using solution casting method. Thin Solid Films. 519, 8375–8378.

Allafchian, A., Jalali, S.A.H., Bahramian, H., Ahmadvand, H., 2016. Preparation, characterization, and antibacterial activity of $NiFe_2O_4$/PAMA/Ag–TiO_2 nanocomposite. J. Magn. Magn. Mater. 404, 14–20.

Aly, K.A., Khalil, N.M., Algamal, Y., Saleem, Q.M.A., 2016. Lattice strain estimation for $CoAl_2O_4$ nano particles using Williamson-Hall analysis. J. Alloys Compd. 676, 606–612.

Bhaumik, A., Shearin, A.M., Patel, R., Ghosh, K., 2014. Significant enhancement of optical absorption through nano-structuring of copper based oxide semiconductors: Possible future materials for solar energy applications. Phys. Chem. Chem. Phys. 16, 11054–11066.

Brintha, S.R., Ajitha, M., 2016. Synthesis, Structural and Antibacterial Activity of Aluminium and Nickel Doped ZnO Nanoparticles by Sol-gel Method. Asian J. Chem. Sci. 1, 1–9.

Cornu, L., Duttine, M., Gaudon, M., Jubera, V., 2014. Luminescence switch of Mn-Doped $ZnAl_2O_4$powder with temperature. J. Mater. Chem. C. 2, 9512–9522.

EL-Moslamy, S.H.,, 2018. Bioprocessing strategies for cost-effective large-scale biogenic synthesis of nano-MgO from endophytic Streptomyces coelicolor strain E72 as an anti-multidrug-resistant pathogens agent. Sci. Rep. 8, 3820.

Geetha Devi, P., Sakthi Velu, A., 2016. Structural, optical and photoluminescence properties of copper and iron doped nanoparticles prepared by co-precipitation method. J. Mater. Sci. Mater. Electron. 27, 10833–10840.

Henari, F.Z., 2001. Optical switching in organometallic phthalocyanine. J. Opt. A: Pure Appl. Opt. 3, 188–190.

Jain, S.R., Adiga, K.C., Pai Verneker, V.R., 1981. A new approach to thermochemical calculations of condensed fuel-oxidizer mixtures. Combust. Flame 40, 71–79.

Karthik, K., Dhanuskodi, S., Gobinath, C., Prabukumar, S., Sivaramakrishnan, S., 2019a. Ultrasonic-assisted CdO–MgO nanocomposite for multifunctional applications. Mater. Technol. 34, 403–414.

Karthik, K., Dhanuskodi, S., Gobinath, C., Prabukumar, S., Sivaramakrishnan, S., 2019b. Fabrication of MgO nanostructures and its efficient photocatalytic, antibacterial and anticancer performance. J. Photochem. Photobiol. B Biol. 190, 8–20.

Karthik, K., Madhukara, N.M., Shashank, M., Vinuth, M., Revathi, V., 2019c. Microwave-Assisted ZrO_2 Nanoparticles and Its Photocatalytic and Antibacterial Studies. J. Clust. Sci. 30, 311–318.

Karthik, K., Vijayalakshmi, S., Phuruangrat, A., Revathi, V., Verma, U., 2019d. Multifunctional Applications of Microwave-Assisted Biogenic TiO_2 Nanoparticles. J. Clust. Sci. 30, 965–972.

Karthik, K., Dhanuskodi, S., Gobinath, C., Prabukumar, S., Sivaramakrishnan, S., 2018. Nanostructured CdO-NiO composite for multifunctional applications. J. Phys. Chem. Solids 112, 106–118.

Karthik, K., Dhanuskodi, S., Gobinath, C., Prabukumar, S., Sivaramakrishnan, S., 2017. Andrographis paniculata extract mediated green synthesis of CdO nanoparticles and its electrochemical and antibacterial studies. J. Mater. Sci. Mater. Electron. 28, 7991–8001.

Manyasree, D., Kiranmayi, P., Ravikumar, R.V.S.S.N., 2018. Synthesis, Characterization and Antibacterial Activity of Aluminium Oxide Nanoparticles. Int. J. Pharm. Pharm. Sci. 10, 32–35.

Mao, Y., Park, T., Wong, S.S., 2005. Synthesis of classes of ternary metal oxide nanostructures. Chem. Commun. 46, 5721–5735.

Mobeen, A., Maria Magdalane, C., Jasmine Shahina, S.K., Lakshmi, D., Sundaram, R., Ramalingam, G., Raja, A., Madhavan, J., Letsholathebe, D., Bashir, A.K.H., Maaza, M., Kaviyarasu, K., 2019. Investigation on antibacterial and photocatalytic degradation of rhodamine-B dye under visible light irradiation by titanium molybdate nanoparticles prepared via microwave method. Surfaces and Interfaces 100381.

Nagaraju, G., Karthik, K., Shashank, M., 2019. Ultrasound-assisted Ta_2O_5nanoparticles and their photocatalytic and biological applications. Microchem. J. 147, 749–754. https://doi.org/10.1016/j.microc.2019.03.094.

Panoiu, N.C., Sha, W.E.I., Lei, D.Y., Li, G.-C., 2018. Nonlinear optics in plasmonic nanostructures. J. Opt. 20, 083001.

Parham, S., Wicaksono, D.H.B., Bagherbaigi, S., Lee, S.L., Nur, H., 2016. Antimicrobial treatment of different metal oxide nanoparticles: a critical review. J. Chinese Chem. Soc. 63, 385–393.

Pathak, N., Gupta, S.K., Sanyal, K., Kumar, M., Kadam, R.M., Natarajan, V., 2014. Photoluminescence and EPR studies on Fe^{3+} doped $ZnAl_2O_4$: an evidence for local site swapping of Fe^{3+} and formation of inverse and normal phase. Dalt. Trans. 43, 9313–9323.

Pathak, T.K., Kumar, A., Swart, C.W., Swart, H.C., Kroon, R.E., 2016. Effect of fuel content on luminescence and antibacterial properties of zinc oxide nanocrystalline powders synthesized by the combustion method. RSC Adv. 6, 97770–97782.

Rithesh Raj, D., Prasanth, S., Vineeshkumar, T.V., Sudarsanakumar, C., 2015. Surface plasmon resonance based fiber optic dopamine sensor using green synthesized silver nanoparticles. Sensors Actuators, B Chem. 224, 600–606.

Sadiq, I.M., Chowdhury, B., Chandrasekaran, N., Mukherjee, A., 2009. Antimicrobial sensitivity of Escherichia coli to alumina nanoparticles. Nanomedicine Nanotechnology. Biol. Med. 5, 282–286.

Sheik-bahae, M., Said, A.A., Van Stryland, E.W., 1989. High-sensitivity, single-beam n_2 measurements. Opt. Lett. 14, 955–957.

Theophil Anand, G., Renuka, D., Ramesh, R., Anandaraj, L., John Sundaram, S., Ramalingam, G., Magdalane, C.M., Bashir, A.K.H., Maaza, M., Kaviyarasu, K., 2019. Green synthesis of ZnO nanoparticle using Prunus dulcis (Almond Gum) for antimicrobial and supercapacitor applications. Surfaces and Interfaces. 17, 100376.

Vijayalakshmi, V., Dhanasekaran, P., 2018. Growth and characterization study of γ-glycine crystal grown using different mole concentrations of zinc sulphate as structure-directing agents. J. Cryst. Growth 498, 372–376. https://doi.org/10.1016/j.jcrysgro.2018.07.013.

Vijayaprasath, G., Murugan, R., Mahalingam, T., Hayakawa, Y., Ravi, G., 2015. Enhancement of ferromagnetic property in rare earth neodymium doped ZnO nanoparticles. Ceram. Int. 41, 10607–10615.

Wang, S.F., Gu, F., Lü, M.K., Cheng, X.F., Zou, W.G., Zhou, G.J., Wang, S.M., Zhou, Y.Y., 2005. Synthesis and photoluminescence characteristics of Dy^{3+}-doped $ZnAl_2O_4$ nanocrystals via a combustion process. J. Alloys Compd. 394, 255–258.

Yadav, S.R., Kuřitka, I., Havlica, J., Hnatko, M., Alexander, C., Masilko, J., Kalina, L., Hajdúchová, M., Rusnak, J., Enev, V., 2018. Structural, magnetic, elastic, dielectric and electrical properties of hot-press sintered $Co_{1-x}Zn_xFe_2O_4$ (x = 0.0, 0.5) spinel ferrite nanoparticles. J. Magn. Magn. Mater. 447, 48–57.

Yugandhar, P., Vasavi, T., Uma Maheswari Devi, P., Savithramma, N., 2017. Bioinspired green synthesis of copper oxide nanoparticles from Syzygiumalternifolium (Wt.) Walp: characterization and evaluation of its synergistic antimicrobial and anticancer activity. Appl. Nanosci. 7, 417–427.

Zare, M., Namratha, K., Alghamdi, S., Mohammad, Y.H.E., Hezam, A., Zare, M., Drmosh, Q.A., Byrappa, K., Chandrashekar, B.N., Ramakrishna, S., Zhang, X., 2019. Novel green biomimetic approach for synthesis of ZnO-Ag nanocomposite; antimicrobial activity against food-borne pathogen, biocompatibility and solar photocatalysis. Sci. Rep. 9, 8303.

Zawadzki, M., 2006. Synthesis of nanosized and microporous zinc aluminate spinel by microwave assisted hydrothermal method (microwave-hydrothermal synthesis of $ZnAl_2O_4$). Solid State Sci. 8, 14–18.

Zhang, B.C., Cao, Y., Zhang, J., Meng, S., Matsumoto, T., Song, Y., Ma, J., Chen, Z., Tatsumi, K., Humphrey, M.G., 2008. Modulation of third-order nonlinear optical properties by backbone modification of polymeric pillared-layer heterometallic clusters. Adv. Mater. 20, 1870–1875.

Zhang, L., Ji, G.F., Zhao, F., Gong, Z.Z., 2011. First-principles study of the structural, mechanical and electronic properties of ZnX_2O_4 (X=Al, Cr and Ga). Chin. Phys. B. 20, 047102.

Zhang, Y.X., Wang, Y.H., 2017. Nonlinear optical properties of metal nanoparticles: A review. RSC Adv. 7, 45129–45144.